Effects of orthogonal cleat structures on hydraulic fracture evolution behavior

Tan, Peng; Fu, Shihao; Huang, Liuke; Chen, Zhaowei; Cao, Jiawei

DOI
10.1016/j.geoen.2024.213119

Publication date
2024

Document Version
Final published version

Published in
Geoenergy Science and Engineering

241 (2024) 213119

Contents lists available at ScienceDirect

Geoenergy Science and Engineering

journal homepage: www.sciencedirect.com/journal/geoenergy-science-and-engineering

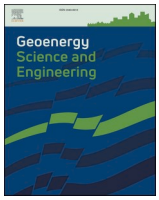

Effects of orthogonal cleat structures on hydraulic fracture evolution behavior

Peng Tan [a,b], Shihao Fu [c], Liuke Huang [d,*], Zhaowei Chen [a,b], Jiawei Cao [a,b]

[a] CNPC Engineering Technology R&D Company Limited, Beijing 102206, China
[b] National Engineering Research Center for Oil & Gas Drilling and Completion Technology, Beijing 102206, China
[c] Delft University of Technology, 2600 AA Delft, The Netherlands
[d] School of Civil Engineering and Geomatics, Southwest Petroleum University, Chengdu, Sichuan 610500, China

ARTICLE INFO

Keywords:
Unconventional reservoir
Hydraulic fracturing
Cohesive zone method
Orthogonal cleat system
Fracture geometries

ABSTRACT

Hydraulic fracturing operation as an effective enhancing coalbed gas production method is widely used in ultra-low permeability coal seam. However, complex geo-stresses and high heterogeneity between natural cleats structure lead to difficulty predicting hydraulic fracture patterns. Fracture evolution behavior for fracturing operation in coal seams requires a better understanding. In this study, a 2D model of hydraulic fracture propagation was built based on the cohesive zone model of finite element method. The effect of orthogonal cleat system, in-situ stress, dig angle and construction parameters on fracture geometries were main investigated. The main conclusions were as follows: (1) According to the interaction types between hydraulic fracture and cleat system, ladder-shaped fracture and H-shaped fracture geometry was summarized. The difference between them was whether there were continuous and small pressure fluctuation stages. (2) When the horizontal stress difference coefficient was lower and larger than 3/12, fracture geometry was prone to present H shape and ladder shape respectively. Besides, the dimensionless fracture length and the dimensionless fracture extension aspect ratio of fracture were increasing with larger horizontal stress difference coefficient. (3) The favorable condition for fracture extension was that the dig angle was 45°. Hydraulic fracture tended to propagate along face cleats direction. (4) Larger fracture fluid displacement was beneficial to form more balanced hydraulic fracture geometry and promote large extension scale. As fracture fluid viscosity increased, the fracture geometries transformed from ladder shape to H shape.

1. Introduction

Hydraulic fracturing as artificial stimulation technology has wide application in ultralow permeability and porosity reservoir. Fracture geometry and extension scale have significant influence on the exploitation of unconventional natural gas, which are also important points for hydraulic fracturing design and optimization, well pattern arrangement and well spacing determination (Cipolla et al., 2010; Huang et al., 2020; Zhang et al., 2022; Feng et al., 2020; Sarkar et al., 2008). Coalbed methane as a typical unconventional gas resource is rich in coalbed reservoir. However, enhancing coalbed gas production through hydraulic fracturing operation faces huge challenges and field problems. Coalbed reservoir as fracture-developed strata, artificial fractures were prone to extended along natural fracture direction, which caused limited fracture extension scale and low single well production Moreover, natural characteristics, such as low hardness, low tensile strength, low permeability and porosity, lead to difficult in fracture extension and limited fracture width (Zhang et al., 2018; Clarkson, 2013; He et al., 2023; Huang et al., 2024).

To better understand the mechanism of evolution of hydraulic fracture in coal seams, the physical and mechanical properties of coal rock has been tested and hydraulic fracture extension models based on experimental and numerical research has been proposed in the recent years. Coalbed reservoir belonged to pores-fracture double medium strata and coal rock had unique orthogonal cleat system through the observation of underground cores (Laubach et al., 1998; Solano-Acosta et al., 2007). The types and distribution of cleat system impacted on mechanical properties and permeability anisotropy. Face cleats and butt cleats were basic fracture types in coal and they were roughly vertical and interconnected with each other. Coalbed methane mainly migrated

* Correspondence author.
E-mail address: swpuhlk@126.com (L. Huang).

https://doi.org/10.1016/j.geoen.2024.213119
Received 24 March 2024; Received in revised form 27 May 2024; Accepted 7 July 2024
Available online 9 July 2024

to the well through face and butt cleats (Fan et al., 2014; Abass et al., 1991). Since the connectivity and density of face cleats were greater than butt cleats, the permeability of face cleats was usually higher than that of butt cleats (Raza et al., 2019). In terms of mechanical properties of coal rock, Li et al. (2000) proved that coal had typical characteristics, such as low elastic modulus, high Poisson's ratio, high brittleness and easily breaking and compressing. Affected by the coal rock size and natural fracture development degree, the experimental results about rock mechanical properties presented large discreteness and obvious anisotropy (Unrug et al., 1985; Huang et al., 2019; Tan et al., 2024). In addition, the uniaxial compressive strength and elastic modulus along face cleats direction was much greater than these along butt cleats direction. Coal metamorphic degree also had certain impact on tensile strength (Wu et al., 2020).

The hydraulic fracture growth in fractured reservoir has been widely studied through physical laboratory experiment. Since fracture extension direction was highly related with natural fracture distribution and density, in-situ stress and rock mechanical properties, the fracture geometries tended to become more complicate, such as T-shaped, offset, branched or multiple fractures (Tan et al. 2017, 2020; Wan et al., 2019; Zou et al., 2016a; Abdelaziz et al., 2023). Abass et al. (1991) found fracture geometry presented multi-branch fracture network connecting cleat system in coal strata instead of single plane fracture. Tan et al. (2019) pointed out that there was high pumping pressure during hydraulic fracturing operation, since lots of pulverized coal migrating into the fracture and multiple fractures near the wellbore, and then these would increase fracturing fluid flow resistance. By using the analogical method, Fan et al. (2014) use concrete material as an analogue for coal rock and found that pumping pressure continued to fluctuate when natural fractures were activated and opened.

In the aspect of numerical modelling, many simulation methods, such as finite element method, extended finite element method, displacement discontinuity method, discrete element method and phase field method, can be used to simulate fracture extension (Khisamitov and Meschke, 2021; Zou et al., 2016b; Tang et al., 2019; Wang et al., 2022; Zheng et al., 2022). Compared with other simulation methods, the cohesive zone model (CZM) as a dominant method in the FEM was employed widely. CZM could simulate fracture evolution by presetting a fracture path zone, whose constitutive model was defined by a traction-separation law. This method could avoid the problem of stress singularity at the fracture tip in linear elastic material (Hwang et al., 2019). Guo et al. (2015) built a 2D fracturing simulation model using CZM to simulate the interaction patterns between artificial fracture and natural fracture. Tan et al. (2021) studied the fracture extension behavior when propagating through transition zone by utilizing the XFEM and CZM. Carrier and Granet (2012) and Wang (2019) developed a tool to realize global zero thickness pore pressure cohesive zone (PPCZ) element, therefore hydraulic fracture could extend along arbitrary direction. However, many numerical studies ignored the effect of cleat systems on fracture extension, resulting in simple and fracture geometries in coal seams.

In this study, a 2D model of hydraulic fracture was built with the consideration of natural fractures in coal seam. The effect of cleat system, in-situ stress, dig angle and construction parameters on fracture patterns were main investigated. In addition, dimensionless fracture length (DFL), dimensionless fracture extension aspect ratio (DFEA) and fracture length were defined to quantitatively analyze fracture propagation characteristics, the fluctuation features of pumping pressure and fracture width of injection node were summarized, according to different hydraulic fracturing operation stage.

2. Methods

2.1. Fluid-solid equations

Rock as a porous medium is composed of rock matrix and pore structure. Equilibrium is expressed by writing the principle of virtual work for the volume, which is shown in Eq. (1) (Reddy, 2019). Fluid is distributed in porous space and fracture void. The continuity equation of fluid flow in porous media is written as Eq. (2) (Zhao et al., 2018). In addition, the fluid flow behavior can be expressed by Darcy's law Eq. (3) (Mohammadnejad and Khoei, 2013).

$$\int_V (\sigma - p_w I)\delta\varepsilon dV = \int_S t\cdot\delta v dS + \int_V f\cdot\delta v dV \tag{1}$$

$$\int_V \frac{1}{J}\frac{\partial}{\partial t}(J\rho_w n_w)dV + \int_V \frac{\partial}{\partial x}\cdot(\rho_w n_w v_w)dV = 0 \tag{2}$$

$$v_w = -\frac{1}{n_w g \rho_w} k\cdot\left(\frac{\partial p_w}{\partial x} - \rho_w g\right) \tag{3}$$

2.2. Constitutive equation of element

The description of rock matrix deformation process can use linear-elastic equation and namely the stress is proportional to the strain. The equitation is showed below:

$$\begin{bmatrix}\varepsilon_x\\ \varepsilon_y\\ \varepsilon_z\\ \gamma_{yz}\\ \gamma_{xz}\\ \gamma_{xy}\end{bmatrix} = \begin{bmatrix}1/E & -\nu/E & -\nu/E & 0 & 0 & 0\\ -\nu/E & 1/E & -\nu/E & 0 & 0 & 0\\ -\nu/E & -\nu/E & 1/E & 0 & 0 & 0\\ 0 & 0 & 0 & -1/G & 0 & 0\\ 0 & 0 & 0 & 0 & -1/G & 0\\ 0 & 0 & 0 & 0 & 0 & -1/G\end{bmatrix}\begin{bmatrix}\sigma_x\\ \sigma_y\\ \sigma_z\\ \tau_{yz}\\ \tau_{xz}\\ \tau_{xy}\end{bmatrix} \tag{4}$$

where E, V, G are elastic modulus, Poisson's ratio and shear modulus. εx, εy, εz and γx, γy, γz are the normal strain and shear strain in three directions.

Before the cohesive element presents damaged condition, the stress-strain relationship is satisfied the following Eq. (5).

$$\begin{bmatrix}\sigma_n\\ t_s\\ t_t\end{bmatrix} = \begin{bmatrix}E_{nn} & E_{ns} & E_{nt}\\ E_{ns} & E_{ss} & E_{st}\\ E_{nt} & E_{st} & E_{tt}\end{bmatrix}\begin{bmatrix}\varepsilon_n\\ \varepsilon_s\\ \varepsilon_t\end{bmatrix} = E\varepsilon \tag{5}$$

where σn, τs and τt are the force applied to cohesive surface in the normal and two shear directions, MPa. εn, εs and εt are the strain in three directions.

2.3. Damage initiation and evolution in cohesive element

As shown in Fig. 1, there are two serial processes in CZM, fracture

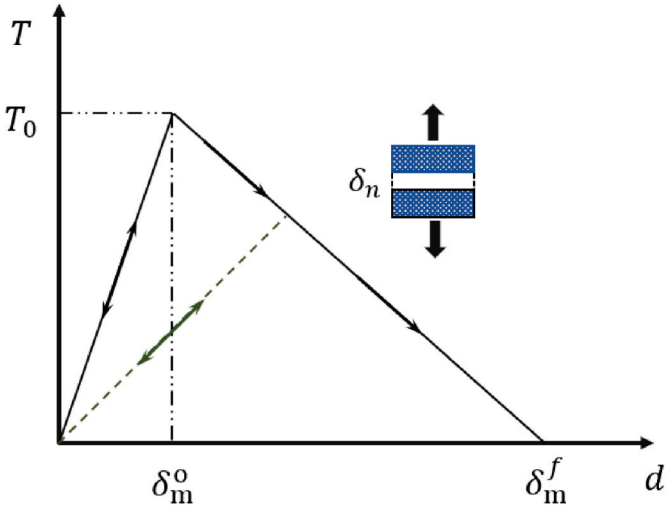

Fig. 1. Damage criterion for cohesive element.

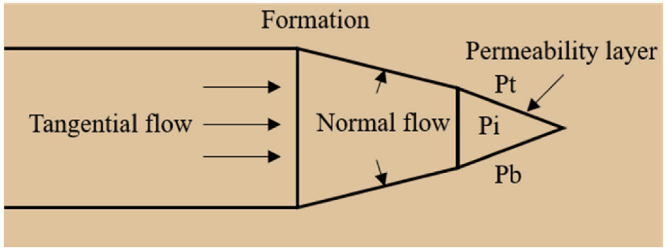

Fig. 2. Demonstration of cohesive zone damage and fluid flow.

initiation and evolution, which is simulated by traction-separation constitutive laws (Zhao et al., 2018).

Maximum nominal stress rule is used to identify whether fracture starts opening or not, which are showed in Eq. (6) and Eq. (7) (Zhao et al., 2018).

$$\max\left\{\frac{\langle\sigma_n\rangle}{\sigma_n^{\max}},\frac{\tau_s}{\tau_s^{\max}},\frac{\tau_t}{\tau_t^{\max}}\right\}=1 \tag{6}$$

$$\langle\sigma_n\rangle=\begin{cases}\sigma_n & \sigma_n\geq 0\\ 0 & \sigma_n<0\end{cases} \tag{7}$$

stiffness evolution of cohesive element can be described as linear loading and linear degeneration, which is showed by Eq. (8) and Eq. (9).

$$\begin{aligned} t_n&=\begin{cases}(1-D)\bar{t}_n & \bar{t}_n\geq 0\\ \bar{t}_n & \bar{t}_n<0\end{cases}\\ t_s&=(1-D)\bar{t}_s\\ t_t&=(1-D)\bar{t}_t\end{aligned} \tag{8}$$

$$D=\frac{\delta_m^f\left(\delta_m^{\max}-\delta_m^o\right)}{\delta_m^{\max}\left(\delta_m^f-\delta_m^o\right)} \tag{9}$$

2.4. Fluid flow in cohesive element

The description of rock matrix deformation process can use linear-elastic equation and namely the stress is proportional to the strain. The equitation is showed below:

Fluid flow process, including tangential flow in fracture void and seepage process from fracture void to rock porous space (Fig. 2), can be summarized by Eq. (10) and Eq. (11), respectively (Gonzalez et al., 2015).

$$q=\frac{w^3}{12\mu}\nabla p \tag{10}$$

$$\begin{cases} q_t=c_t(p_i-p_t)\\ q_b=c_b(p_i-p_b)\end{cases} \tag{11}$$

3. Model establishment and verification

3.1. Model establishment

Cleats were extremely developed in coal seams and there was huge difference between the butt and face cleats in the aspect of mechanical properties. To investigate the influence of cleat system on fracture geometry evolution, butt and face cleats was assigned different mechanical parameters. Then the effect of in-situ stress, dig angle, pumping rate, fluid viscosity and cleats on the initiation and propagation of hydraulic fracture were studied. The model was composed of rock matrix, butt and face cleats (Fig. 3). The size of fracturing model was 20*20 m, and butt and face cleats were orthogonal to each other.

In this work, the perforation site was simulated by initial damaged element at the center part of injection node. Therefore, fracture initiated from the perforation point and propagated along the cleats path. The rock elements were presented by solid element CPE4P, which could simulate solid deformation and fluid seepage process. The mesh diagram with the value dig angle of 45° is shown in Fig. 4(a). The cleat system was set as the cohesive element, which was meshed as COH2D4P element, 4823 units totally. Fig. 4(b) shows the top view of different element combination. Cohesive elements (COH1, COH2 and COH3) preset in rock solid elements (E1, E2, E3, E4 and E5) were used to simulate face cleats and butt cleats. It is worthy to point out that middle nodes in cohesive elements should be merged at intersection point, which makes pressure continuity in face cleat element and butte cleat elements. Therefore, this method can simulate fracture penetration and branch behavior. In addition, Ux(X = 0) = Ux(X = 20) = 0 and UY(Y = 0) = UY(Y = 20) = 0 meant that the displacement of X-components and Y-components at the boundary surface being zero. Effective stress rules were adopted for whole formation pressure system, therefore the stress applied to rock matrix was equal to geo-stress minus the product of pore pressure and Biot coefficient.

3.2. Model parameters

Previous studies showed that the tensile strength and fracture toughness had significant impact on fracture extension (Awaji and Sato, 1978). These parameters could give a basic reference to build simulation model. Therefore, natural field rocks were trimmed to different size cores for Brazilian disk splitting test (BDST) and Straight-notched Brazilian disc test (SNBD).

The BDST was conducted with 25 mm in diameter and 5 mm in thickness sample. During the test, the sample was loaded along diameter direction of disc until the splitting failure occurred. The indirect tensile strength of coal rock could be calculated by Eq. (12) from the standard

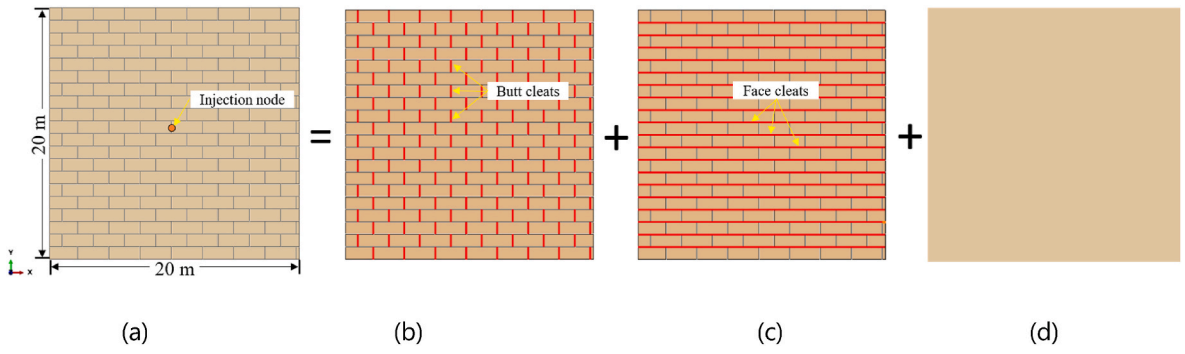

Fig. 3. The diagram of numerical model with 0 dig angle. (a) Diagram of the model and the orange point is the injection node; The red lines in (b) and (c) represent the cleat system; (d) Rock matrix.

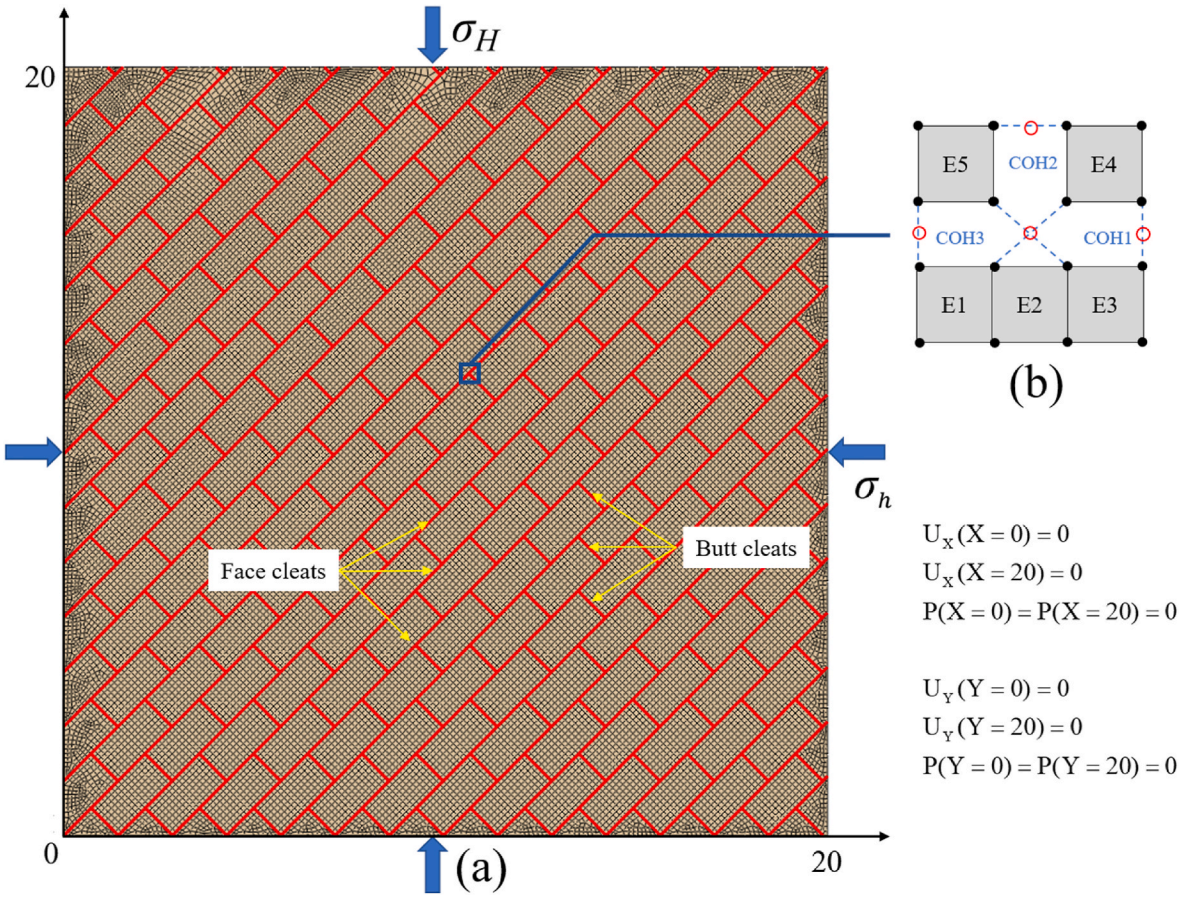

Fig. 4. Schematical representation of the orthogonal cleat system with 45o dig angle (The angle between the minimal horizontal principal stress and face cleats in coal rock). (a) The position of butt cleats and face cleats, (b) Intersection point in the connection of cohesive element.

method of ISRM (Bieniawski and Hawkes, 1978). The experimental procedure of SNBD was similar to BDST. The sample of BDST was trimmed to a disc with a diameter of 50 mm firstly, then 8 mm or 10 mm of crack was preset in the central part of samples. The angle between loading direction and preset crack presented 30°. The II-type fracture toughness was obtained by Eq. (13) (Atkinson et al., 1982). The results of BDST and SNBD is showed in Table 1. The average of the tensile strength and fracture toughness in coal is 0.74 MPa and 0.16 MPa•m1/2, respectively. In addition, the hardness of coal was measured by hardness tester and the average value is 20.96 kg/mm2. Overall, coal rock was a typical low tensile strength, low fracture toughness and low hardness material. Based on experimental results, the simulation model parameters are showed in Table 2.

$$S_t = 2P/(\pi dl) \tag{12}$$

$$K = P\sqrt{a}N/\left(\sqrt{\pi}RB\right) \tag{13}$$

Table 1
BDST and SNBD test results.

BDST test results		SNBD test results		
Load/ *KN*	Tensile strength/*MPa*	Fracture length/*mm*	Load/ *KN*	Fracture toughness/ *MPa·m*^{½}
0.072	0.350	8	0.32	0.145
0.175	0.850	10	0.382	0.187
0.247	0.989	10	0.289	0.149

3.3. Model verification

In order to validate the simulation method, a 2D hydraulic fracture extension simulation model was built (Fig. 5(a)). The simulation parameters were below: the elastic modulus and Poisson's radio are 20 GPa and 0.2 respectively. The value of fracture fluid viscosity and displacement were 0.1 Pa s and 0.002 m^3/s, and the total calculating time was 100 s. Since the CZM solution was compared with analytic solution of KGD model, the influence of in-situ stress on fracture extension was ignored in calculating process. In addition, hydraulic energy was mainly dissipated in the opening of fracture and friction loss of fracturing fluid, and the fluid viscosity was usually large in field operation. Therefore, the methods of comparison mainly focused on the impact of fracturing fluid viscosity on fracture extension. The comparison of fracture width of injection point between the KGD model and simulation model is presented in Fig. 5(b). The average value difference between two models was smaller than 5% and it validated this simulation method.

4. Results and analysis

4.1. Hydraulic fracture geometry in coal seams

Under the observation of simulation results, 2D fracture extension path was not always present a single straight line with impact of the distribution of cleat faces, the difference of in-situ stress, the displacement and viscosity of fracturing fluid. Normally, fracture geometries showed non-linear extension path with the opening of weak structural planes. Therefore, two typical geometry evolutions of hydraulic fracture under different situations were summarized according to the extension path characteristic. The process of different types of fracture extension is

Table 2
Numerical model parameters.

Categories	Parameters	Value
Rock matrix	Elastic modulus, E *(GPa)*	5.344
	Poisson's ratio, v	0.345
	Permeability coefficient, k *(m/s)*	1.5×10^{-6}
	Void ratio	0.1
Face cleat	Critical normal stress, σ_n^{max} *(MPa)*	0.972
	First direction shear stress, τ_n^{max} *(MPa)*	8
	Second direction shear stress, τ_t^{max} *(MPa)*	8
Butt cleat	Critical normal stress, σ_n^{max} *(MPa)*	0.517
	First direction shear stress, τ_n^{max} *(MPa)*	8
	Second direction shear stress, τ_t^{max} *(MPa)*	8
In-situ stress	Maximal horizontal principal stress, σ_H *(MPa)*	11~12
	Minimal horizontal principal stress, σ_h (MPa)	11
Pumping Parameters	Fluid viscosity, μ *(Pa•s)*	0.01
	Injection rate, q *(m^3/s)*	0.01–0.1
Initial conditions	Leakoff coefficient, C *(m/Pa·s)*	1×10^{-14}
	Pore pressure, P_o *(MPa)*	10
	Biot coefficient, α	0.8

shown in Fig. 6.

(1) Ladder shaped fracture: Hydraulic fracture initiated from the injection node on the butt cleats and propagated along the σH firstly. Then the fracture extended to the face cleats and formed a small shaped fracture (Fig. 6(a1)). After that, hydraulic fracture communicated butt cleats and face cleats in turn (Fig. 6(a2-a7)). Finally, the ladder shaped fracture was formed after several extension direction turns (Fig. 6(a8)).
(2) Asymmetry H shaped fracture: Hydraulic fracture initiated from the injection node and propagated along butt cleats (Fig. 6(b1)), and then hydraulic fracture connected butt and face cleats and present symmetrical pattern (Fig. 6(b2-b4)). While the injection of fracturing fluid, the fracture began to show the characteristics of non-conforming propagation (Fig. 6(b5-b7)). Ultimately, the fracture geometry presented asymmetry shape (Fig. 6(b8)).

4.2. Characteristics of pump pressure curve

The injection pressure curves and fracture width of injection node are shown in Fig. 7. According to the fracture evolution features, fracture propagation process of the hydraulic fracture can be divided in to three stages.

(1) Energy accumulation

Hydraulic fracture initiated at the injection node and fracturing fluid began to enter and gradually filled in the pores and formation. At this stage of a-b, fracture propagated along the butt cleats and the pressure curve presented small fluctuation, since the fracture extended to the intersectional area between butt cleats and face cleats. After that, hydraulic fracture turned its extension direction and propagated along the face cleats. Since face cleats had large critical normal stress value, the opening of face cleats needed more hydraulic energy. When sufficient pressure of fluid in the fracture void, face cleats were opened and then communicated by the hydraulic fracture. The accumulation of pressure process is shown in H stage (a-c).

(2) Pumping pressure decreasing

Beyond peak pressure (point c), the fracturing fluid gradually enriched into the face cleats, and injection pressure decreased at the minimum point as it reached the point of d. The decrease of pressure process is shown in H stage (c-d). The bifurcation of hydraulic fracture and opening face cleats needed more hydraulic energy. When fracture turned the extension direction smoothly, the pumping pressure in the injection node decreased immediately.

(3) Formation of different shape fracture

At this stage (d-e), ladder shaped fracture and asymmetry H shaped fracture showed different characteristics. During the process of ladder shaped fracture, the fluid pressure was re-accumulated and pressurized with continuous fluid injection. When the fluid pressure was sufficient to overcome the interfacial tension of butt cleats, butt cleats could be activated and opened. Then the pressure of injection point dropped again. The pressure of injection point fluctuated frequently resulting from the effect of fracture extension direction turning. The hydraulic fracturing pressure and fracture width of injection node were increasing dramatically. During the extension process of asymmetry H shaped fracture, the pressure curve in III stage was smoother and stabler than that of ladder shaped fracture, because fracture propagated along the face cleats horizontally and artificial fracture would not connect butt cleats. The bottomhole pressure and fracture width had little increase and stay relative stable.

5. Analysis of influencing factors on hydraulic geometry

5.1. Effect of cleat system

The existence of highly developed natural weak surface such as cleat

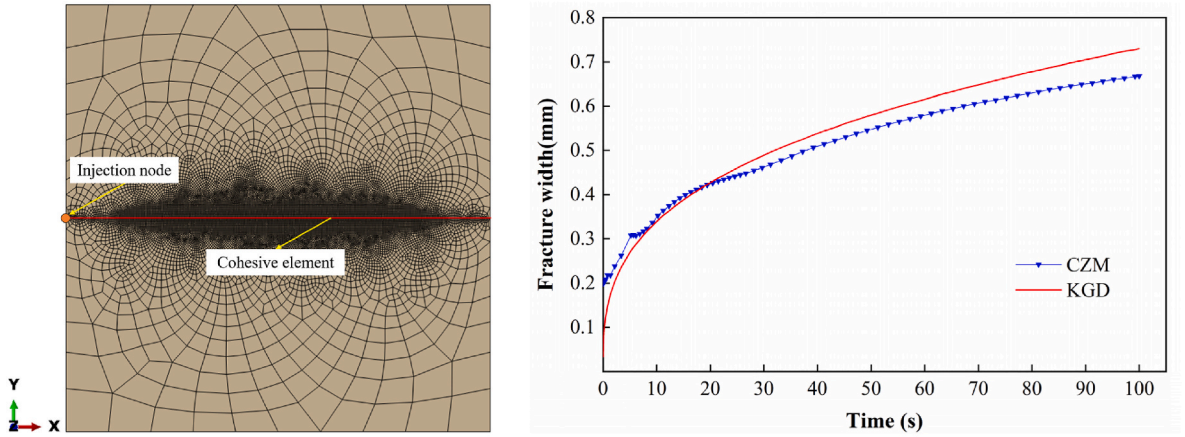

(a) The sketch of simulation model (b) Fracture width in injection point

Fig. 5. The validation of CZM.

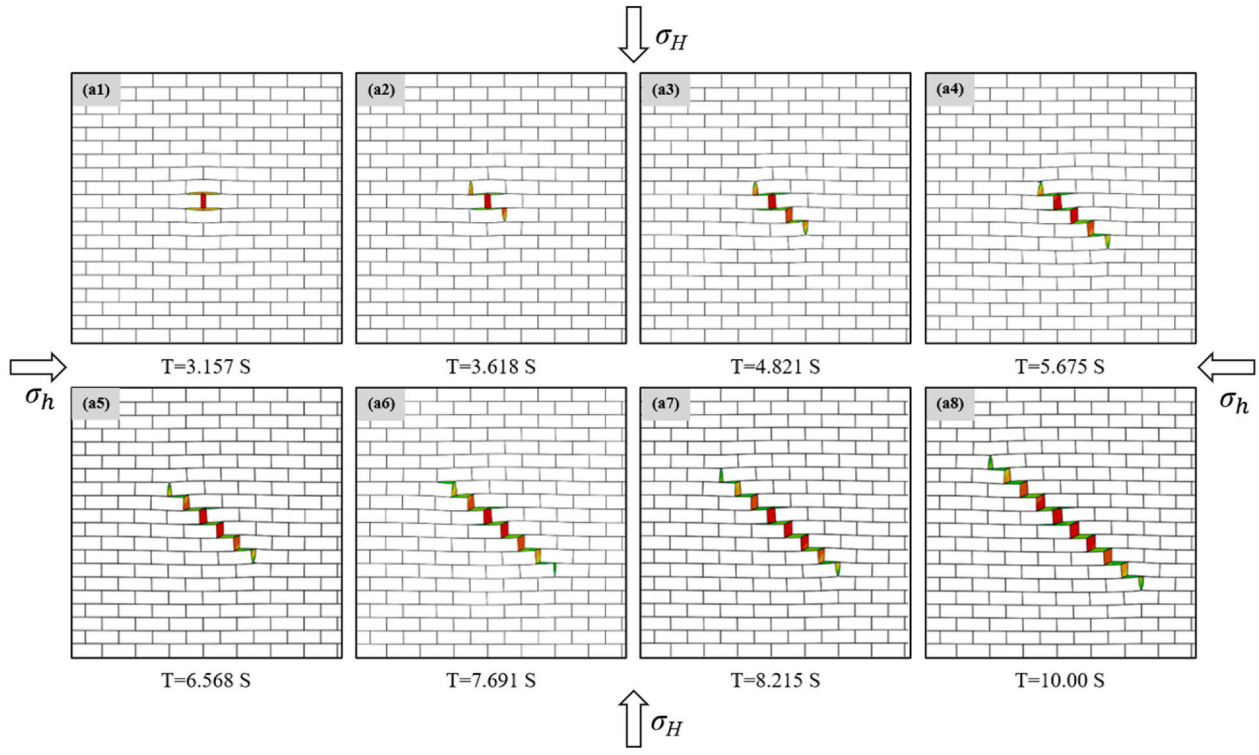

(a) Ladder shaped fracture

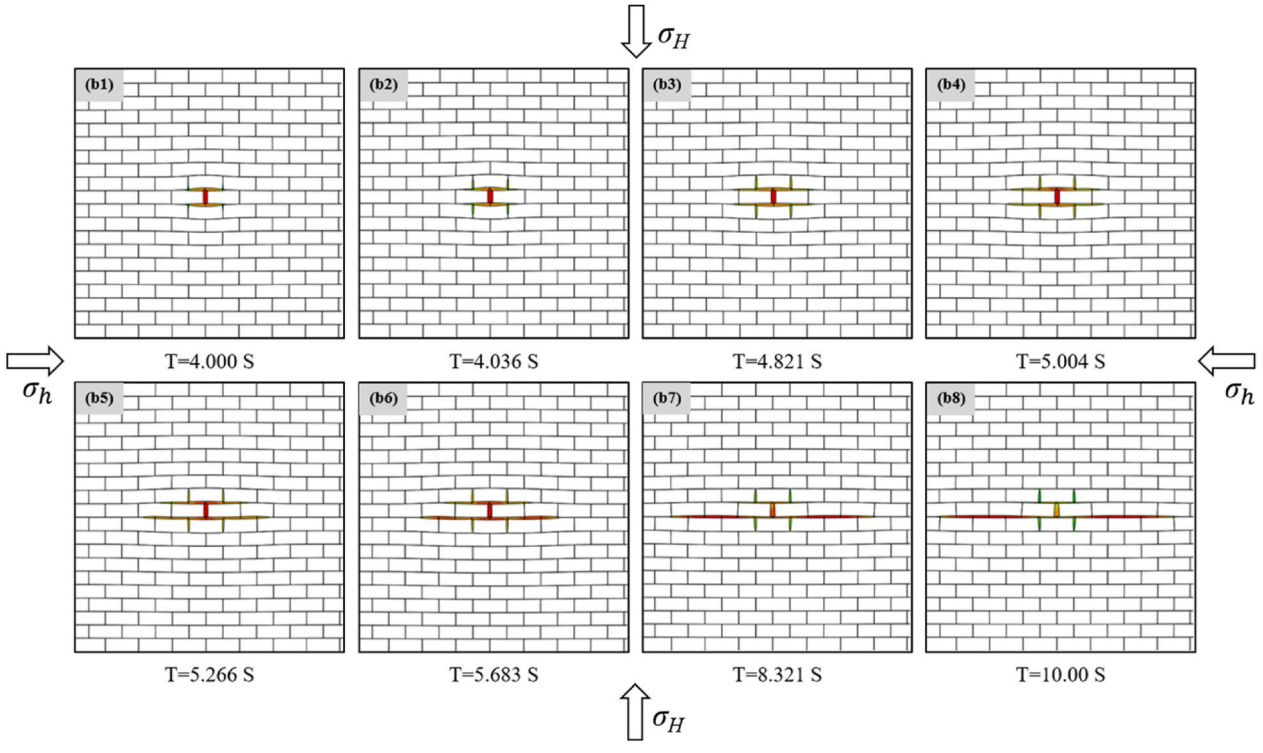

(b) H shaped fracture

Fig. 6. (a1)-(a8) and (b1)-(b8) show the ladder shaped fracture and H shaped fracture extension process.

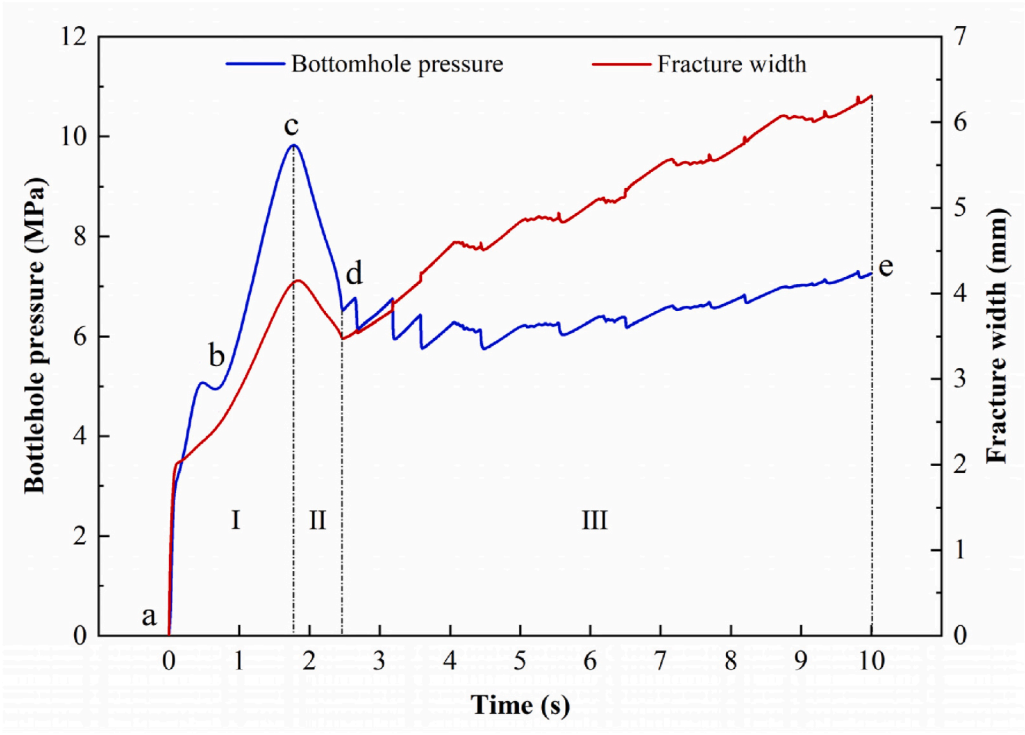

(a) Ladder shaped fracture

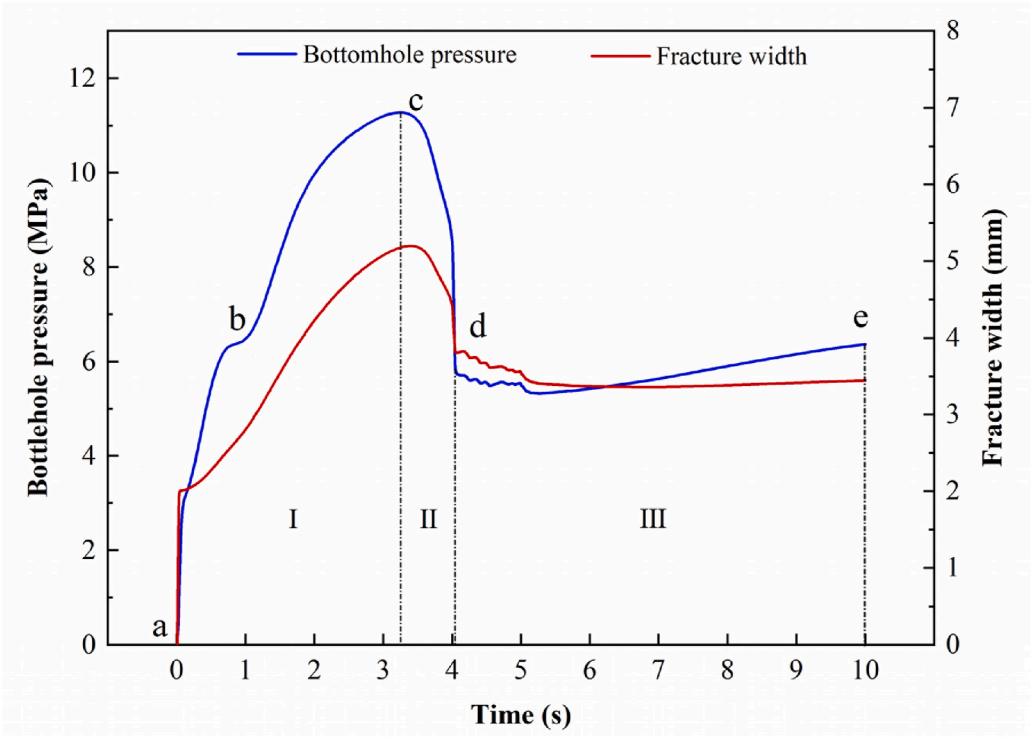

(b) H shaped fracture

Fig. 7. (a) and (b) represented the bottom hole pressure and fracture width in different types of fracture geometries.

system, bedding planes was the prerequisite condition to realize the effective development of unconventional reservoir. Butt cleats and face cleats were interlaced in coal rock, and opening different kinds of natural weak surface needed different hydraulic energy. This was the reason why the ultimate fracture geometry presents abnormal complicated and diverse characteristic.

Natural weak fracture was an advantage for forming complex fracture network in unconventional reservoir. The cohesive strength of cleat system, tensile and shear strength of coal rock was much smaller than these of rock matrix (Zhao et al., 2018). In this study, hydraulic fracture had the tendency to propagate along the natural weak fracture path rather than propagate in rock matrix, and the fracture extension direction was prone to steer and bifurcate (See Fig. 8), which showed that hydraulic fracture extension direction was not always parallel to the maximum horizontal principal stress direction. In addition, mechanical property such as tensile strength and fracture energy difference was not only reflected in rock matrix and natural fracture surface, but also in butt cleats and face cleats. Therefore, there was a different difficulty between butt cleats and face cleats to be opened and activated. Summarily, hydraulic fracture easily propagated along the direction of minimal tensile strength and fracture energy, and hydraulic fracture extension law was followed to the principle of minimal flow resistance, minimal energy dissipation and shortest propagation path. Thus, it was necessary to explore the distribution of natural weak fracture and test the mechanical strength of weak surface. On the base of above, it is beneficial to design the hydraulic fracturing operation plan with largest stimulated stimulate reservoir and ultimate gas production.

5.2. Effect of in-situ stress

In-situ stress condition was one of the predominate factors to determinate the ultimate hydraulic fracture geometry in coal gas reservoir. The influence of horizontal in-situ stress on hydraulic fracture initiation and propagation could be attributed to horizontal geo-stress difference coefficient. The coefficient can be expressed as the ratio of the difference between the maximum and the minimum horizontal principal stress to the minimum horizontal principal stress (See Eq. (14)). There are six different horizontal in-situ stress difference coefficients were set in the numerical simulation.

$$K_H = \frac{\sigma_H - \sigma_h}{\sigma_h} = \frac{\Delta\sigma}{\sigma_h} \tag{14}$$

The simulation results showed that horizontal principal stress difference coefficient induced hydraulic fracture steering and bifurcating and the evolution of hydraulic fracture extension direction would influence the ultimate hydraulic fracture extension scale and fracture length. The direction turning degree and expanding range of hydraulic fracture were different with different in-situ stress. With low horizontal principal stress difference coefficient value, hydraulic fracture pattern presented H shape and mainly connected face cleats. As the value increased, hydraulic fracture type was changed from H shape to ladder shape and turned extension direction many times (see Fig. 9).

Fracture length along butt cleat direction and fracture extension scale were two major indicators to describe hydraulic fracture propagation geometry. To summarize the impact of horizontal stress difference on hydraulic fracture patterns, two dimensionless parameters were defined: dimensionless fracture length (DFL) and dimensionless fracture extension aspect ratio (DFEA).

Dimensionless fracture length = fracture length along butt cleat direction / simulation model length

Dimensionless fracture extension aspect ratio = accumulated activating butt cleats length / accumulated activating face cleats length

The DFL could be used to describe the degree of fracture extension direction change. The large value of DFL meant that fracture extension direction change more frequently and fracture mainly connect butt cleats. The DFEA ratio was to describe the equilibrium of hydraulic fracture growth pattern. That the value was much closer to one showed that hydraulic fracture propagated with more balanced way. The impact of horizontal stress difference on DFL and DFEA ratio is present in Fig. 10. The results showed that when the horizontal stress difference coefficient was smaller than 2/12, the DFL and DFEA ratio had the smaller value. DFL and DFEA are increasing with increase of horizontal stress difference coefficient increased. Therefore, under low horizontal stress difference coefficient, the fracture extension patterns were mainly affected by the mechanical properties of cleat system. Under high value situation, the fracture propagation behavior was dominated by horizontal stress difference.

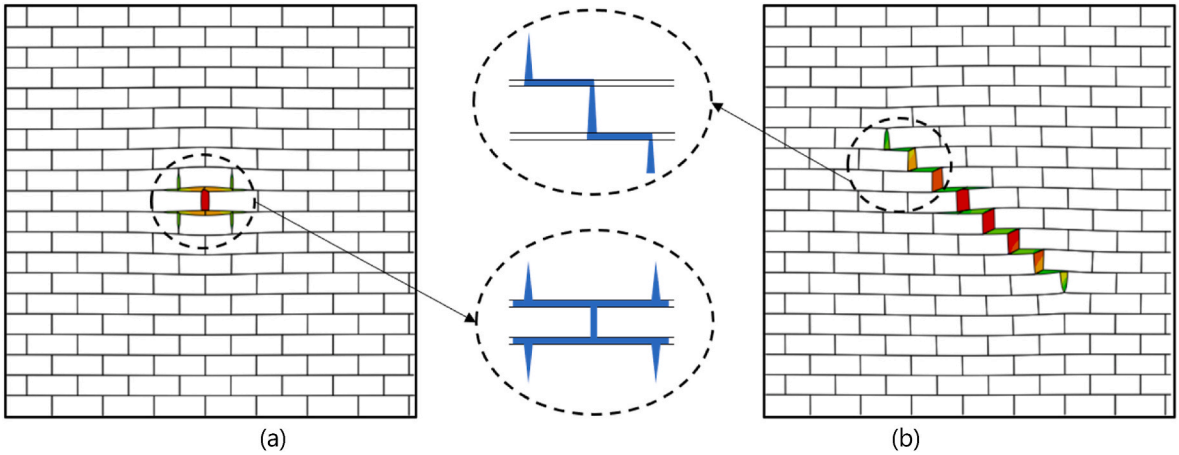

Fig. 8. The burification and steering of hydraulic fracture in (a) and (b) respectively.

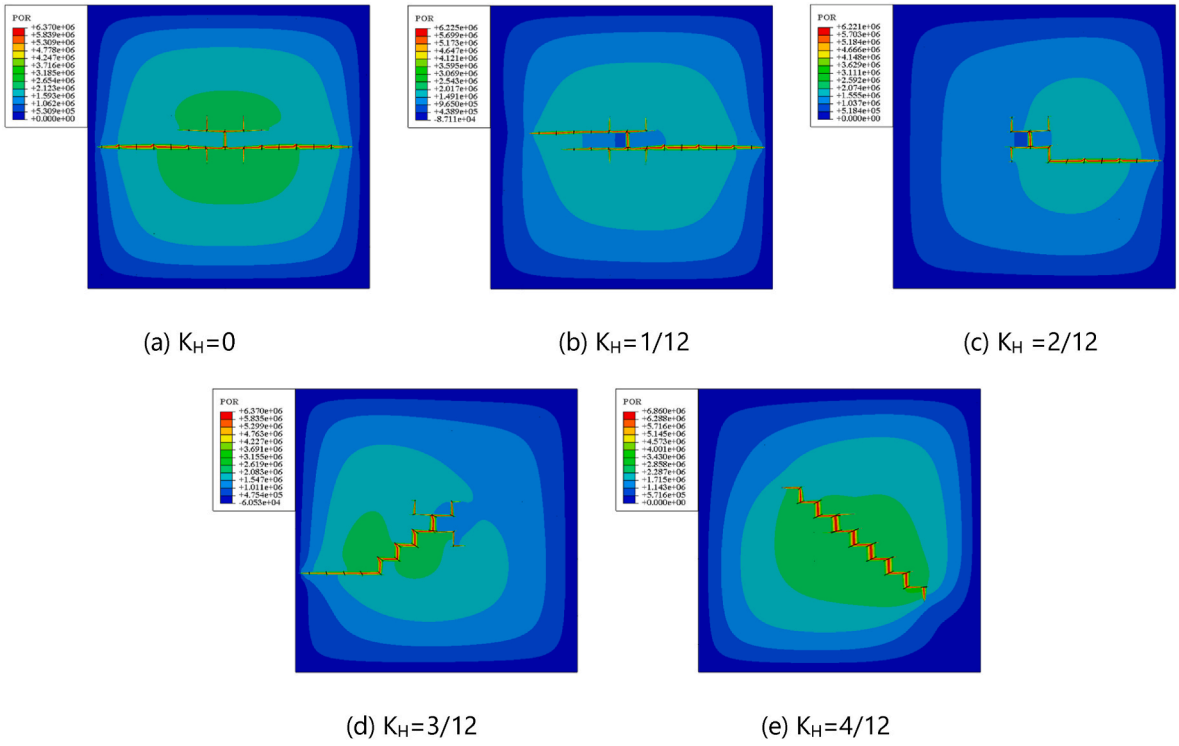

Fig. 9. The fracture geometry with different K_H values.

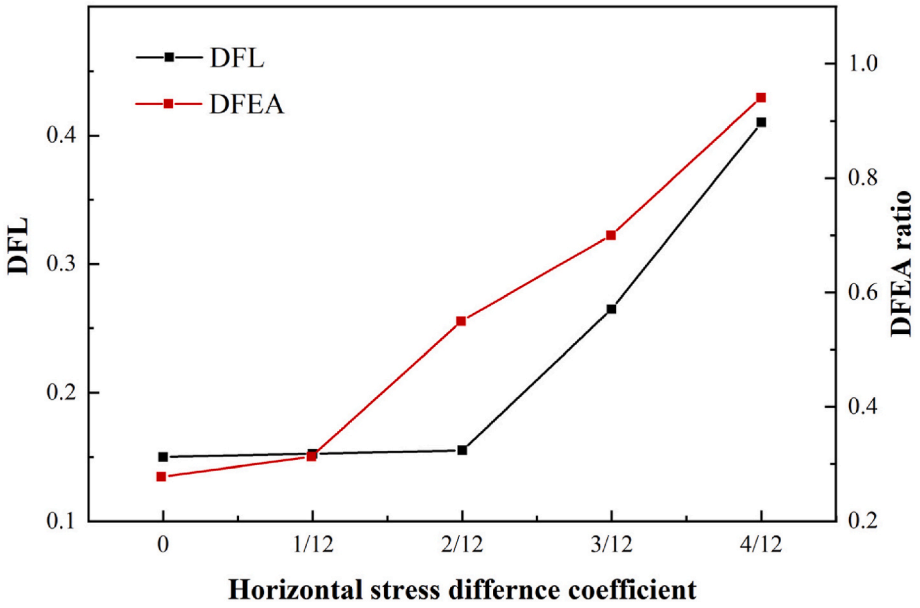

Fig. 10. The DFL and DFEA radio under different stress difference coefficient.

5.3. *Effect of dig angle*

The distribution of natural fracture in reservoir affected the hydraulic fracture propagation way and ultimate extension scale. Previous study was mainly focused on the interaction type and propagation criterion of one hydraulic fracture and one natural fracture. However, natural weak surfaces in coal rock were developed. Therefore, it is necessary to consider the impact of natural fracture group distribution on hydraulic fracture extension geometry. The dig angle was especially defined as dig angle between the face cleat and minimal horizontal principal stress (See Fig. 11). Three dig angles were set as 0°, 45° and 90° to investigate the effect of dig angle on fracture patterns.

As the simulation results were showed in Fig. 11, hydraulic fracture extension direction was affected by the combined influence of in-situ stress and natural fracture group. The possibility of hydraulic fracture propagating along the face cleats increased with dig angle increasing. When dig angle was 0o, the possibility of fracture extension direction along face cleats or butt cleats were almost similar. When the value was 90°, fracture mainly extended along face cleats direction, also the maximum horizontal principal stress direction. The ultimate fracture length was short in 90° dig angle, since there was no the effect of butt cleats during propagation. In conclusion, the most advantageous dig

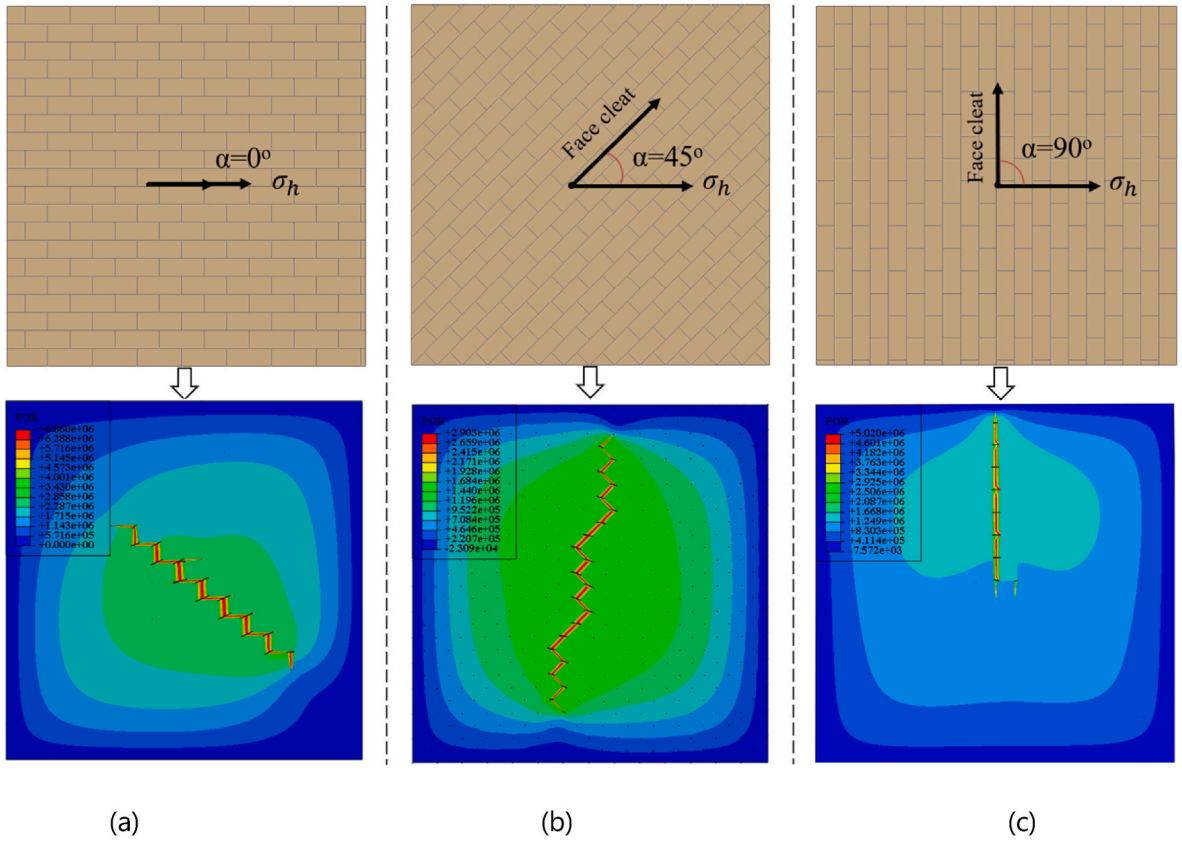

Fig. 11. The simulation results of 0°, 45° and 90° dig angle are shown in (a), (b) and (c).

angle for creating hydraulic fracture length was 45°. Under the condition of natural fracture group distribution and in-situ stress direction, hydraulic fracture had the tendency to propagate along face cleats direction, and activated more butt cleats as the same time, thus the largest fracture length could be formed in this situation.

5.4. Effect of injection rate and fluid viscosity

Injection rate and fluid viscosity were the significant construction parameters in hydraulic fracturing operation design. Field operation experiment showed that high displacement and high viscosity were beneficial to form single and straight hydraulic fracture geometry

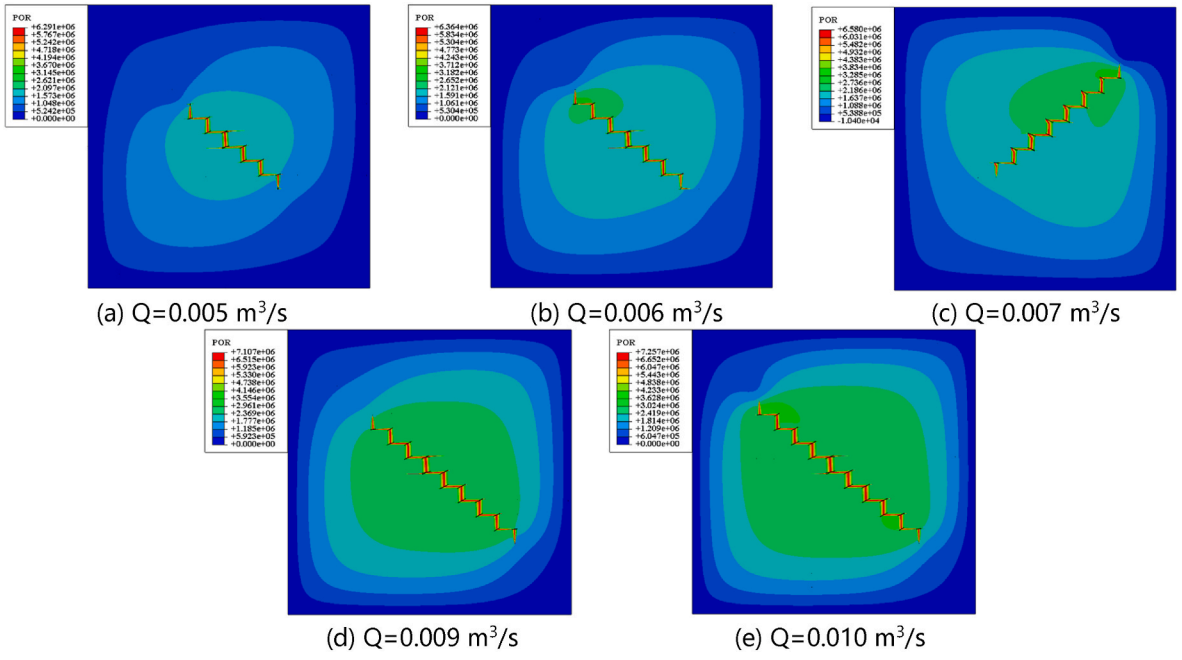

Fig. 12. The fracture geometries under different injection rate.

instead of complex fracture network in dense reservoir. However, it was difficult to form long main hydraulic fracture in coal gas reservoir, since there are numerous natural fractures. Therefore, different injection rates and viscosity of fracturing fluid were set in this section and the effect of engineering parameters on fracture extension area and fracture patterns were main investigated.

The fracture patterns with different pump rate are shown in Fig. 12. As the increase of injection rate from 0.005 m^3/s to 0.010 m^3/s, the fracture extension scale became larger and extension geometry kept constant. The possible reason was that high injection rate meant that pressure could be accumulated at fracture tips and the chance of fracture opening was much larger. It has little influence on fracture extension direction change and then fracture patterns keep same type. The fracture geometry with different fracturing fluid viscosity is presented in Fig. 13. When the viscosity ranges from 0.01 Pa s to 0.05 Pa s, there was no huge change in the fracture geometry and fracture extension scale, but when the value was beyond 0.10 Pa s, the fracture geometry turned to unsymmetric H-shape fracture, which meant that viscosity of hydraulic fluid affected the fracture extension direction, since hydraulic fracture extension law was obeyed to the lowest resistance. Normally Stimulated Reservoir Volume (SRV) or Stimulated Reservoir Area (SRA) are used to evaluate the process of hydraulic fracturing in 3D space (Hou et al., 2014; Wei et al., 2017). Because of the 2D numerical model, the fracture length evolution as time with different factors is employed to evaluate the hydraulic fracture extension scale. The results of fracture length in different displacement and fluid viscosity are shown in Fig. 14. It is worthy to point out that there were initial damage cohesive elements, so hydraulic fracture length started non zero value. The fracture length presented a positive correlation with injection rate and was negative correlation with fluid viscosity. The larger displacement meant that more hydraulic energy could be used to open natural fracture. When fluid viscosity increased and flow resistance in fracture was larger, therefore the hydraulic energy which should have been used for opening new fracture were employed for overcoming flow friction resistance.

6. Discussion

(1) Bedding planes and cleat system were extremely developed in coal gas reservoir. The tensile and shear strength of these weak structures were far lower than that of rock matrix. Hydraulic fractures were prone to open natural fracture, turn their extension direction and induce lots of fracture fluid filtration. As the fluid was injected into formation, the pressure in hydraulic fracture increased and fractures could communicate with farther weak planes. Therefore, the existence of natural fracture and its complex degree could induce hydraulic fracture propagation. In addition, the difficulty degree of fracture extension was related with the type of natural fracture and distribution structure. Different from bedding planes in shale rock, the coal measure strata showed strong heterogeneity in the interlayer and interface, since natural fracture types included face cleats and butt cleats. In terms of structure, face cleats and butt cleats were perpendicular or nearly perpendicular to each other. There was huge difference in physical property and mechanical parameters between two directions. On the basis of above analysis, the effect of different factors on fracture extension in coal was mainly studies in this paper. The result showed that when the angle between in-situ stress and face cleats was 45o, hydraulic fracture geometry presented "zigzag" extension model and mainly extended along the face cleat direction, which had the same conclusion compaered with Olsen et al. (2003) (See Fig. 15(a)). Both of them formed "zigzag" hydraulic fracture, which validated the accuracy of simulation method. In addition, Massarotto et al. (2003) calculated the permeability anisotropy degree of coal rock in horizontal plane and found that permeability difference between plane cleat and end cleat was up to 6:1. The effect of permeability difference between face cleat and butt cleat on fracture extension could be considered in further study. In addition, due to the calculating capacity limitation, the fracture extension in height direction was ignored in this paper. Therefore, it was necessary to study fracture propagation in three dimensions scale in coal seams.

(2) To further study the hydraulic fracture geometry in coal measure reservoir, the simulated coal rock sample was made by pouring concrete into a 300 mm*300 mm*300 mm cube mould. With the consideration of well-developed face cleat and butt cleat in coal rock, two groups of orthogonal cemented fractures were made.

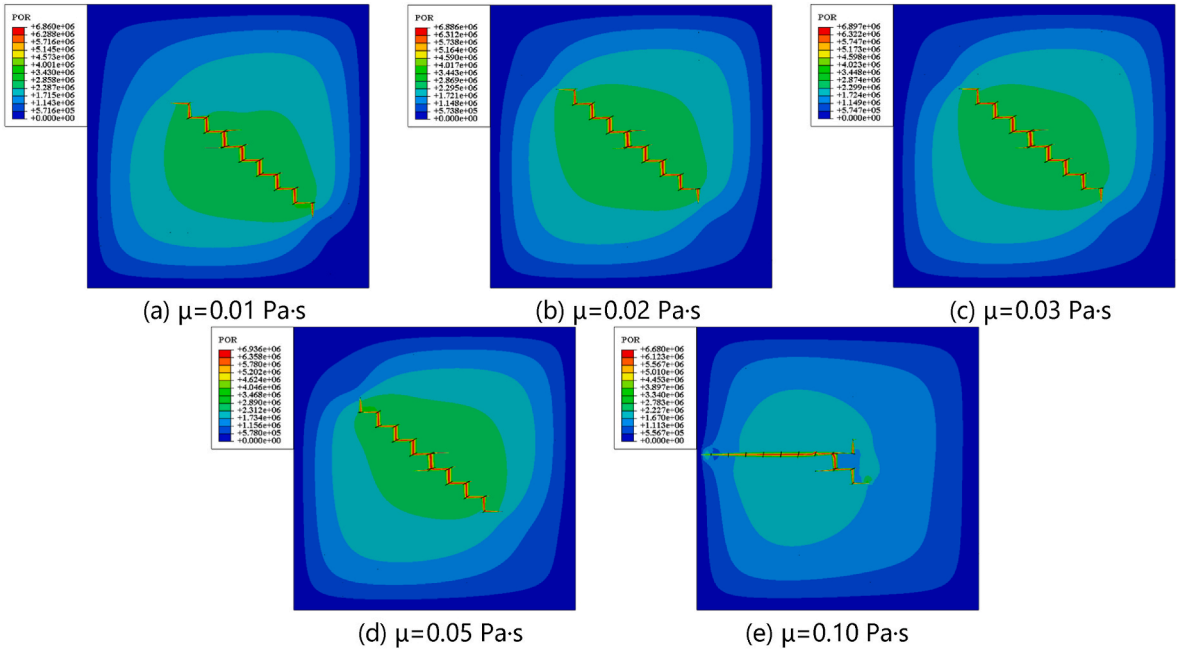

Fig. 13. The fracture geometries under different fluid viscosity.

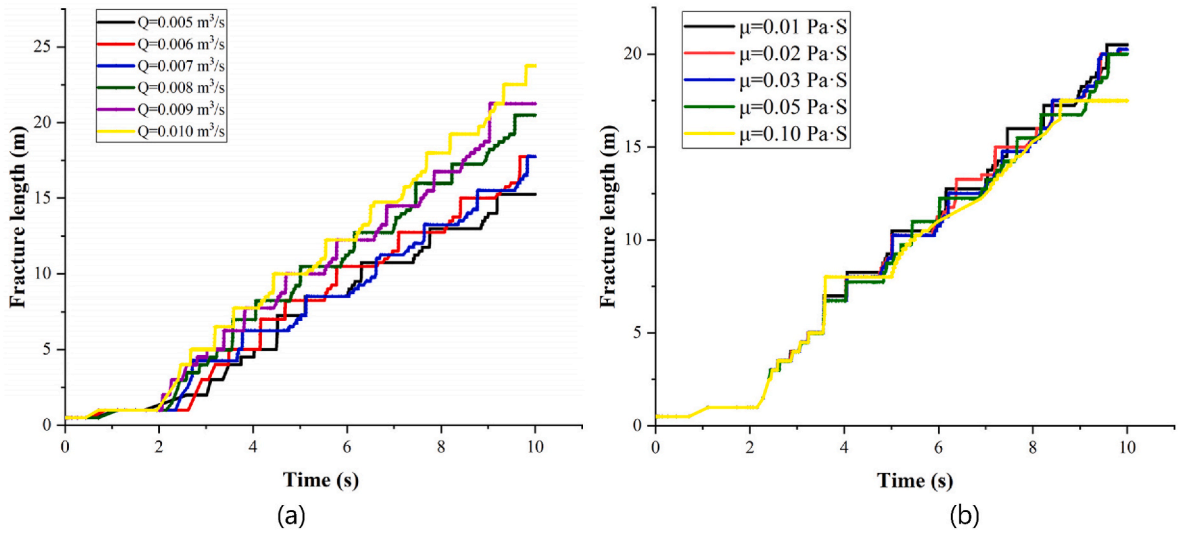

Fig. 14. The fracture length in different injection rate and fluid viscosity.

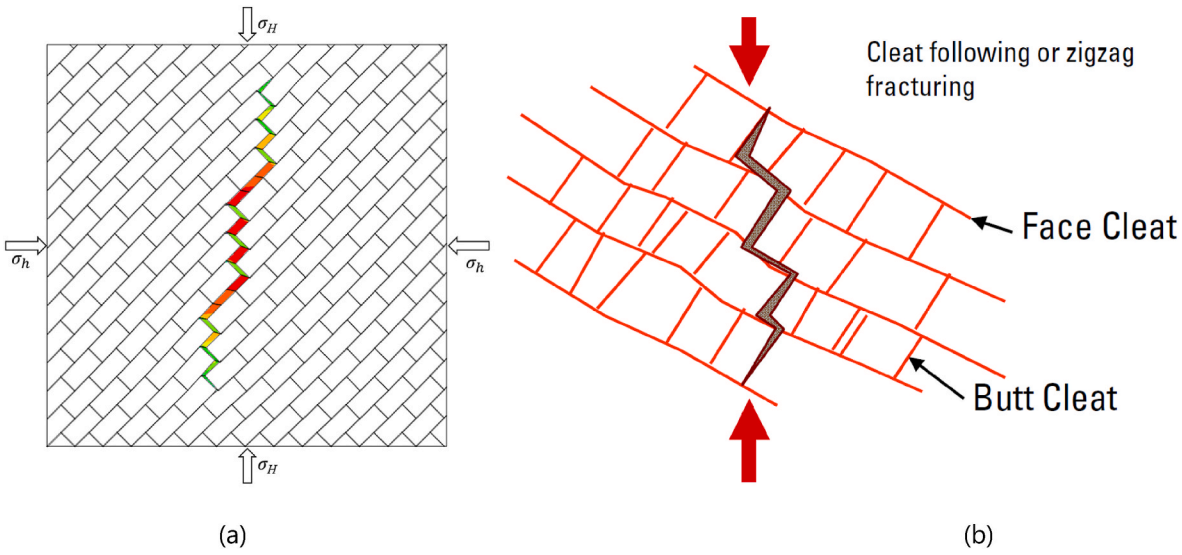

Fig. 15. Complex fracture geometry where maximum stress is at an angle to face cleats. (a) Simulation result, (b) The diagram of hydraulic fracture patterns in coal (Olsen et al., 2003).

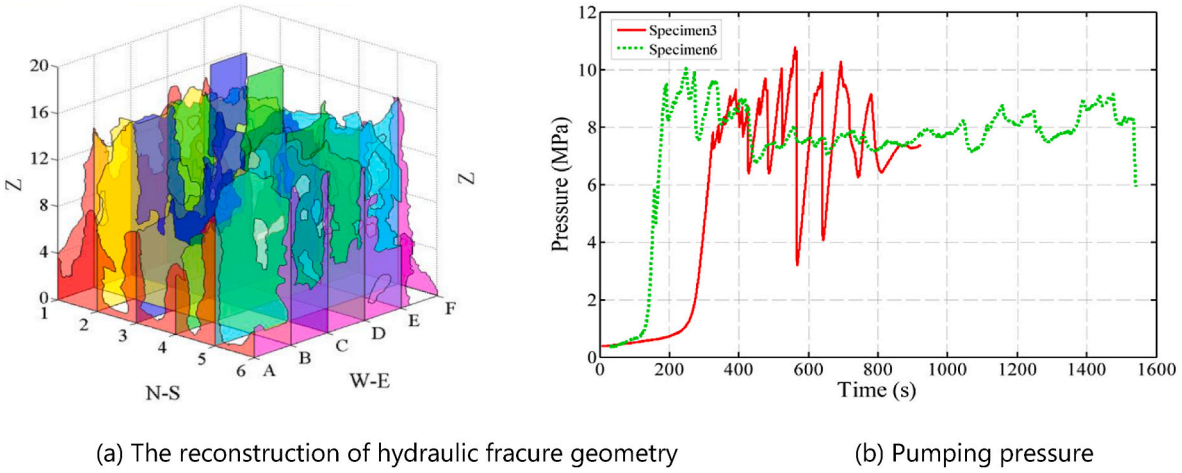

Fig. 16. The tri-axial experiment of coal rock (Fan et al., 2014).

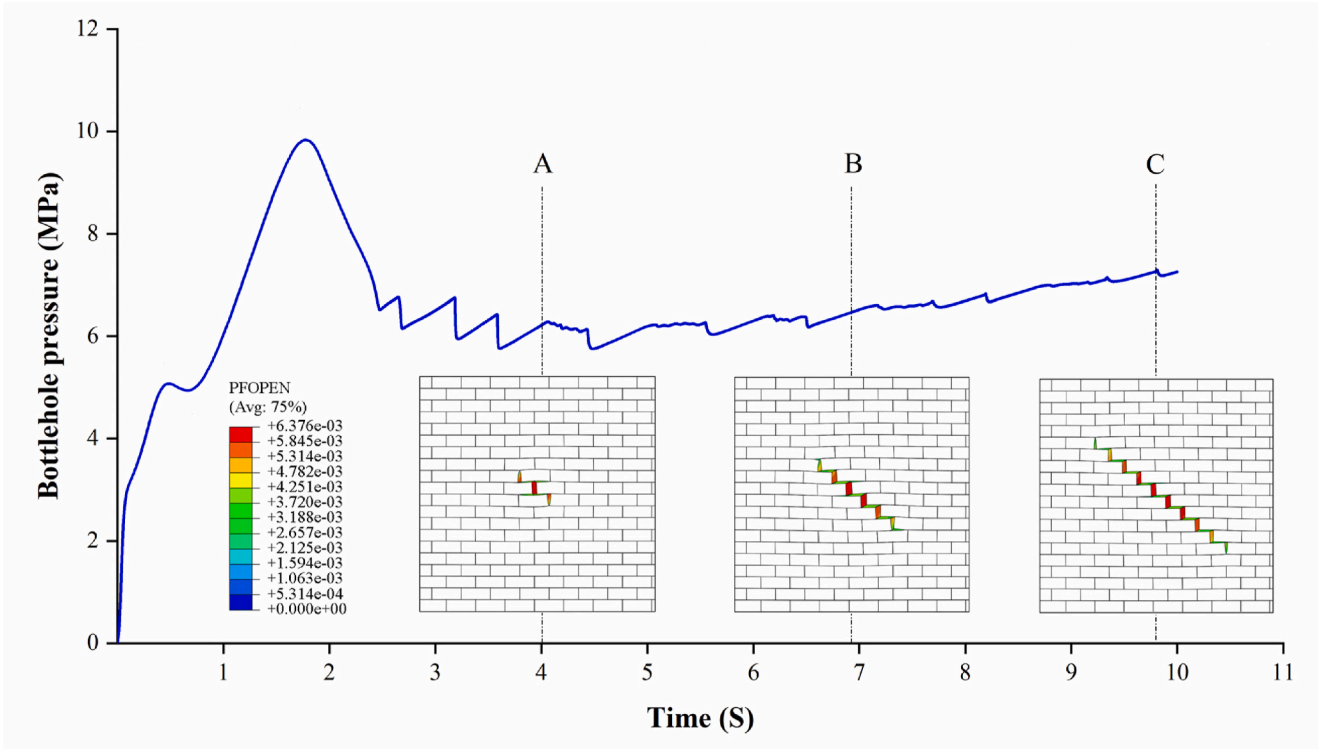

(a) The pumping pressure of ladder shaped fracture. Pressure fluctuates many times in stage of A-C

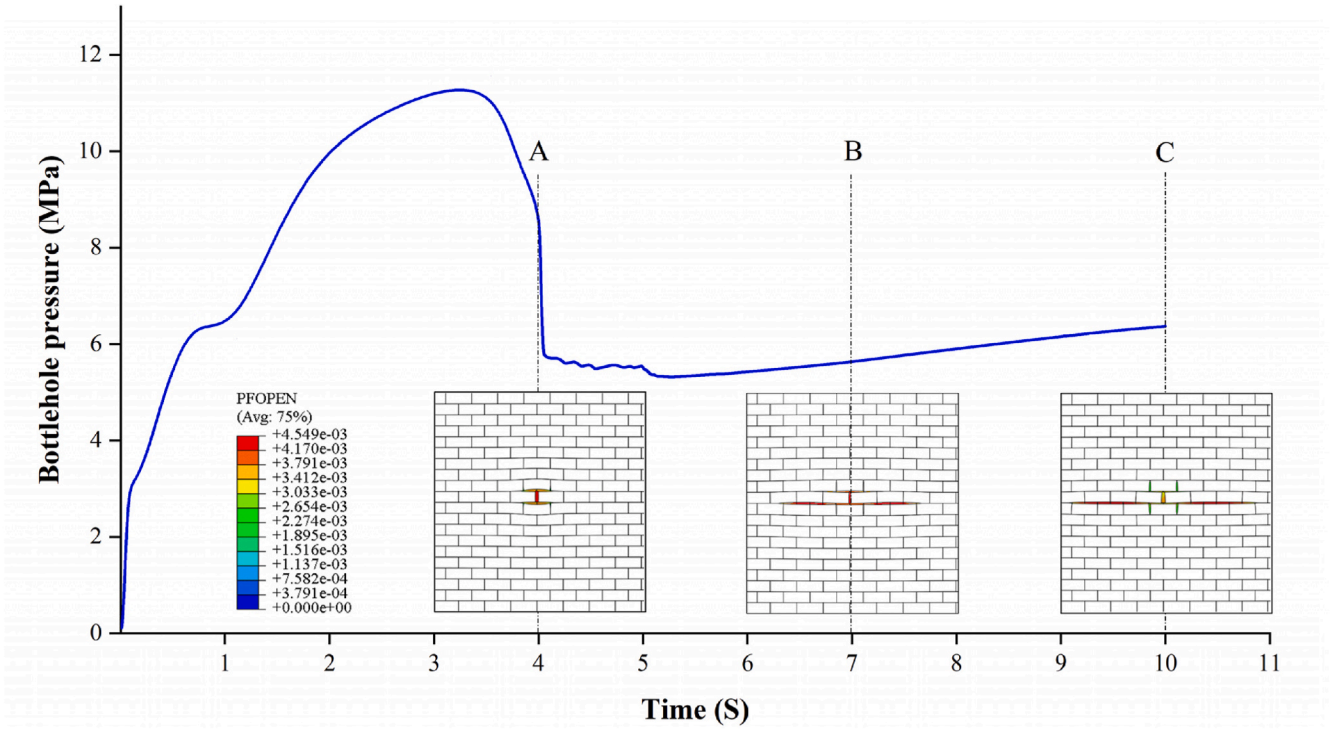

(b) The pumping pressure of H shaped fracture. Pressure curve increases steadily in stage of A-C

Fig. 17. The pumping pressure curve.

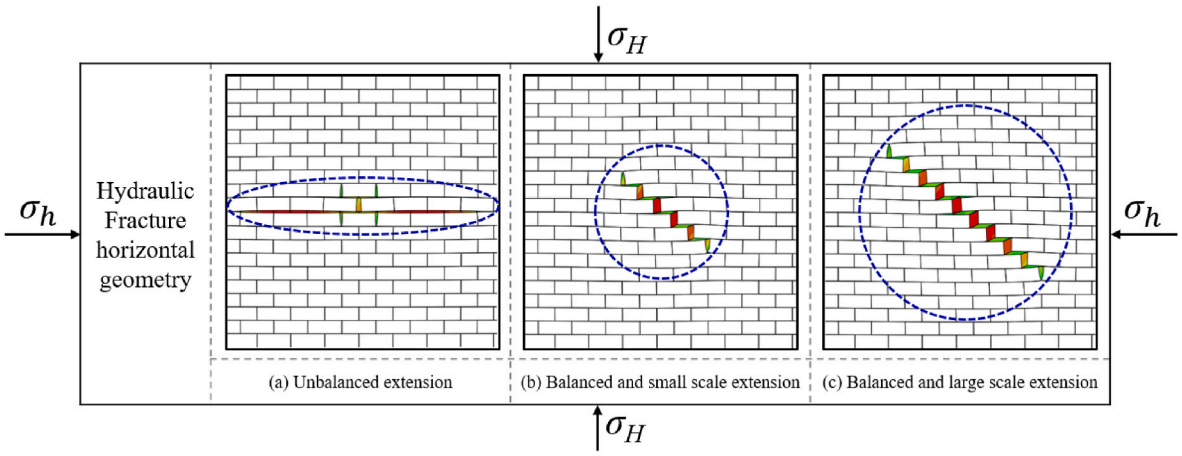

Fig. 18. Hydraulic fracture geometry in horizontal plane.

The true triaxial hydraulic fracturing test system was used to conduct experiment (Fan et al., 2014). Fluorescent tracer was added into fracturing fluid was convenient to easily observe hydraulic fracture propagation geometry, when splitting the specimen along the crack surface after experiment. The results showed that the hydraulic fracture patterns presented non-plane expansion and opening with weak structural plane. In order to observe the hydraulic fracture geometry in three dimensions, the fracture extension path was rebuilt according to the fluorescent tracer distribution (See Fig. 16(a)). Surface with different color showed that the orthogonal cleat system was continuously active or opened. The result of experimental and numerical research in the study showed that fracture propagated tortuously in horizontal plane and the natural fracture could induce the diversion and branch of fracture, which could enhance the complexity of hydraulic fracture network. On the other hand, the hydraulic fracturing fluid loss increased and the hydraulic energy was dissipated.

(3) The difference between ladder shaped fracture and H shaped fracture was whether there were continuous small pressure fluctuation stages during hydraulic fracture connected natural fracture. The pumping pressure of ladder shaped fracture is presented in Fig. 17(a). When hydraulic fracture communicated the cleat system in coal rock (A-C), there were many "increase-drop-increase" stages in the pressure curve. It was considered that when ladder fracture was connecting natural weak surfaces, the diversion of fracture in horizontal plane needed more hydraulic energy. Besides that, the opening of new fracture and direction change of fracture joint distributed of the whole hydraulic energy. The accumulation and release of hydraulic fracture in fracture tip led to the fluctuation in pumping pressure curve. Under the condition of H shaped fracture, there was no change of hydraulic fracture extension direction between face cleat and butt cleat, and pumping pressure increased steadily. (See Fig. 17 (b)). In the filed operation, coal powder was easily mixed with hydraulic fracturing fluid and then formed paste, which possibly blocked the fracture channel of coalbed methane migration, increased the flow resistance and enhanced the hydraulic fracture pressure. When pressure could accumulate a certain high value, the hydraulic energy was enough to break through the blocking zone and hydraulic fracture could extend further. Therefore, the construction pressure also tended to show many wave curves of "increase-drop-increase" fluctuation in coal gas reservoir. Combined with the pressure curve in triaxial hydraulic fracturing experiment, there was several minutes of pressure fluctuation stage (See Fig. 16(b)), which had high agreement with numerical study results. The fracture extension patterns and the connecting degree between artificial fracture and natural fracture could be judged by pressure fluctuation characteristic in coal gas reservoir, which also gives a good guidance to hydraulic fracturing operation.

(4) The long support artificial fracture and large seepage area during fracturing operation were beneficial to effectively enhance the oil and gas production. Therefore, the balanced extension and propagation scale of hydraulic fracture was vital to hydraulic fracturing operation design. According to the lowest energy principal, the hydraulic fracture was prone to extend along the maximum horizontal principal stress in homogenous rock. However, there were many natural weak structures in coal, the extension path of fracture was not always along the maximum horizontal principal stress. Based on above analysis, three types of hydraulic fracture geometry in coal rock were summarized (See Fig. 18). Unbalanced extension mode presented that fracture propagation ability in one certain direction was much larger than other directions, which led to hydraulic fracture could effectively connect the natural fractures. Balanced extension mode was showed in Fig. 18(b–c), the fracture extension capacity in maximum or minimum principal horizontal stress direction kept the same level. But the extension scale was different between each other, since the displacement in (c) was larger than that in (b). The balanced extension fracture geometry and large stimulated reservoir area were desired to be formed in field operation. Thus, it was not only necessary to survey the in-situ stress condition in advance, but also to obtain the distribution and strike of cleat surface, which was helpful for hydraulic fracture activating natural fractures. In addition, suitable enhancement of injection rate could enlarge the hydraulic fracture extension area in coal gas reservoir.

7. Conclusions

The numerical experiments were conducted to simulate the evolution of hydraulic fracture in coal seams. The effect of cleat system, in-situ stress, dig angle and construction parameters on fracture geometries were main studied. The main conclusions were as follows.

(1) Cleats surfaces significantly influenced the hydraulic fracture extension direction. According to the interaction types between hydraulic fracture and cleat system, two types of typical hydraulic fracture geometries were found, including ladder shaped

fracture and H shaped fracture. The difference between two types fracture was whether there were continuous small pressure fluctuation stages when connecting face cleats and butt cleats.

(2) The ultimate fracture patterns in coal gas reservoir were different under different in-situ stress conditions. When the horizontal stress difference coefficient was lower than 3/12, the fracture geometry was prone to present ⊥ shaped fracture. When larger than 3/12, the ladder shaped fracture was formed. In addition, the dimensionless fracture length and the dimensionless fracture extension aspect ratio of fracture was increasing with larger horizontal stress difference coefficient.

(3) The distribution of cleats structure in coal seams had a great impact on the formation of complex fracture network. The favorable condition to fracture extension was that the dig angle was 45°. Hydraulic fracture had the tendency to propagate along face cleats direction and activated more butt cleats meanwhile.

(4) Larger fracture fluid displacement was beneficial to form balanced and large extension scale hydraulic fracture geometry. As the increase of fracture fluid viscosity, hydraulic fracture geometries transformed from ladder shape to H shape.

CRediT authorship contribution statement

Peng Tan: Investigation. **Shihao Fu:** Methodology. **Liuke Huang:** Methodology. **Zhaowei Chen:** Validation. **Jiawei Cao:** Writing – review & editing.

Declaration of competing interest

The authors declare that they have no known competing financial interests or personal relationships that could have appeared to influence the work reported in this paper.

Data availability

No data was used for the research described in the article.

Acknowledgments

The authors sincerely appreciate the funding provided by CNPC Science and Technology Project (Grant No. 2021DQ03-37, and No. 2022DJ8005), the National Natural Science Foundation of China (Grant No. 52334001, and No. 42372337), Natural Science Starting Sroject of SWPU (No. 2022QHZ009).

Nomenclature

S_t= tensile strength, MPa
P= applied radial force, N
d= diameter of rock sample, mm
l= core length, mm
K= fracture toughness, MPa·m$^{1/2}$
P= loading pressure, Pa
α= half of prefabricated fracture length, mm
N= dimensionless stress intensity factor
R= sample radius, mm
B= sample thickness, mm
σ= effective stress skeleton of rock, Pa
δ_e= virtual strain rate tensor, S^{-1}
δ_v= virtual velocity, m/s
t= surface force, N/m^2
f= volume force, N/m^3
J= formation volume change rate, dimensionless
n_w= void radio
ρw= fracturing fluid density, Kg/m^3
vw= fluid velocity, m/s
k= permeability matrix, m/s
g= gravitational acceleration vector, m/s^2
To= critical stress, Pa
δ_m^o= separation reaches the critical value, m
σn= tensile stress of the normal direction applied to the cohesive element surface, MPa
τs and τt= shear strengths, MPa
σ_n^{max}, τ_n^{max} and τ_t^{max}= critical failure stress, MPa
$\overline{t_n}$ $\overline{t_s}$ and $\overline{t_t}$= stress components predicted by the elastic traction-separation behavior for the strains without damage
D= dimensionless damage factor
δ_m^f= distance when the cohesive element is fully damaged, m
δ_m^{max}= maximum value of the effective separation during the loading period, m
δ_m^o= displacement of unit node when the cohesive element begins to be damaged, m
q= volume flow, m^3/s; w - fracture width, m; μ - fluid viscosity, Pa•s
P= pressure in the hydraulic fracture, Pa
q_t and q_b= flow rates filtrating to the formation with different surface, m/s
c_t and c_b= loss coefficients, m/(Pa•s)
P_i= fluid pressure in the fracture, Pa
P_t, P_b= pore pressure with top and bottom surface, Pa

References

Abass, H.H., Hedayati, S., Kim, C.M., 1991. Mathematical and experimental simulation of hydraulic fracturing in shallow coal seams. In: Paper Presented at the SPE Eastern Regional Meeting, Lexington, Kentucky. https://doi.org/10.2118/23452-MS. SPE-23452- MS.

Abdelaziz, A., Ha, J., Li, M., 2023. Understanding hydraulic fracture mechanisms: from the laboratory to numerical modelling. Advances in Geo-Energy Research 7 (1), 66–68. https://doi.org/10.46690/ager.2023.01.07.

Atkinson, C., Smelser, R.E., Sanchez, J., 1982. Combined mode fracture via the cracked Brazilian disk test. Int. J. Fract. 18 (4), 279–291. https://doi.org/10.1007/BF00015688.

Awaji, H., Sato, S., 1978. Combined mode fracture toughness measurement by the disk test. ASME J. Eng. Mater. Technol. 100 (2), 175–182. https://doi.org/10.1115/1.3443468.

Bieniawski, Z.T., Hawkes, I., 1978. Suggested methods for determining tensile strength of rock materials. Int. J. Rock Mech. Min. Sci. Geomech. Abstr. 15 (3), 99–103.

Carrier, B., Granet, S., 2012. Numerical modeling of hydraulic fracture problem in permeable medium using cohesive zone model. Eng. Fract. Mech. 79, 312–328. https://doi.org/10.1016/j.engfracmech.2011.11.012.

Cipolla, C.L., Warpinski, N.R., Mayerhofer, M.J., 2010. The relationship between fracture complexity, reservoir properties, and fracture treatment design. In: Paper Presented at the SPE Annual Technical Conference and Exhibition, Denver, Colorado, USA, vol. 25, pp. 438–452. https://doi.org/10.2118/115769-MS, 04.

Clarkson, C.R., 2013. Production data analysis of unconventional gas wells: workflow. Int. J. Coal Geol. 109–110, 147–157. https://doi.org/10.1016/j.coal.2012.11.016.

Fan, T., Zhang, G., Cui, J., et al., 2014. The impact of cleats on hydraulic fracture initiation and propagation in coal seams. Pet. Sci 11 (4), 532–539. https://doi.org/10.1007/s12182-014-0369-7.

Feng, Q.H., Xu, S.Q., Xing, X.D., et al., 2020. Advances and challenges in shale oil development: a critical review. Advances in Geo-Energy Research 4 (4), 406–418. https://doi.org/10.46690/ager.2020.04.06.

Gonzalez, M., Taleghani, A.D., Olson, J.E., 2015. A cohesive model for modeling hydraulic fractures in naturally fractured formations. SPE Hydraulic Fracturing Technology Conference. The Woodlands, Texas, USA. https://doi.org/10.2118/SPE-173384-MS. SPE-173384-MS.

Guo, J., Zhao, X., Zhu, H., et al., 2015. Numerical simulation of interaction of hydraulic fracture and natural fracture based on the cohesive zone finite element method. J. Nat. Gas Sci. Eng. 25, 180–188. https://doi.org/10.1016/j.jngse.2015.05.008.

He, R., Yang, J., Li, L., et al., 2023. Investigating the simultaneous fracture propagation from multiple perforation clusters in horizontal wells using 3D block discrete element method. Front. Earth Sci. 11, 1–19. https://doi.org/10.3389/feart.2023.1115054.

Hou, B., Chen, M., Li, Z.M., et al., 2014. Propagation area evaluation of hydraulic fracture networks in shale gas reservoirs. PETROL EXPLOR DEV+ 41 (6), 763–768. https://doi.org/10.1016/S1876-3804(14)60101-4.

Huang, L., Liao, X., Fan, M., et al., 2024. Experimental and numerical simulation technique for hydraulic fracturing of shale formations. Adv. Geo-Energy Res. 13, 83–88. https://doi.org/10.46690/ager.2024.08.02.

Huang, L.K., Liu, J.J., Zhang, F.S., et al., 2019. Exploring the influence of rock inherent heterogeneity and grain size on hydraulic fracturing using discrete element modeling. INT J SOLIDS STRUCT 176, 207–220. https://doi.org/10.1016/j.ijsolstr.2019.06.018.

Huang, L.K., Liu, J.J., Zhang, F.S., et al., 2020. 3D lattice modeling of hydraulic fracture initiation and propagation for different perforation models. J. Petrol. Sci. Eng. 191, 107169 https://doi.org/10.1016/j.petrol.2020.107169.

Hwang, J., Manchanda, R., Sharma, M.M., 2019. An extended finite volume model for implicit cohesive zone fracture propagation in a poroelastic medium. COMPUT METHOD APPL M 350, 571–594. https://doi.org/10.1016/j.cma.2019.03.040.

Khisamitov, I., Meschke, G., 2021. Variational interface element model for 2d and 3d hydraulic fracturing simulations. COMPUT METHOD APPL M 373, 113450. https://doi.org/10.1016/j.cma.2020.113450.

Laubach, S.E., Marrett, R.A., Olson, J.E., et al., 1998. Characteristics and origins of coal cleat: a review. Int. J. Coal Geol. 35 (1–4), 175–207. https://doi.org/10.1016/S0166-5162(97)00012-8.

Li, Z.G., Fu, S.L., Wu, X.L., et al., 2000. Research on mechanical property test and mechanism of hydraulic fracture of gas well in coal beds. Petroleum Drilling Techniques 28 (3), 10–13.

Massarotto, P., Rudolph, V., Golding, S.D., 2003. Anistropic permeability characterisation of permian coals. International Coalbed Methane Symposium.

Mohammadnejad, T., Khoei, A.R., 2013. An extended finite element method for hydraulic fracture propagation in deformable porous media with the cohesive crack model. Finite Elem. Anal. Des. 73, 77–95. https://doi.org/10.1016/j.finel.2013.05.005.

Olsen, T.N., Galen, B., Taryn, F., 2003. Improvement processes for coalbed natural gas completion and stimulation. In: Paper Presented at the SPE Annual Technical Conference and Exhibition. https://doi.org/10.2118/84122-MS. Denver, Colorado. SPE 84122.

Raza, S.S., Ge, L., Rufford, T.E., et al., 2019. Anisotropic coal permeability estimation by determining cleat compressibility using mercury intrusion porosimetry and stress–strain measurements. Int. J. Coal Geol. 205, 75–86. https://doi.org/10.1016/j.coal.2019.02.011.

Reddy, J.N., 2019. Introduction to the Finite Element Method, fourth ed. McGraw-Hill Education, New York.

Sarkar, A., Ali, M., Sagar, R., et al., 2008. Cleat characterization in CBM wells for completion optimization. In: Paper Presented at the SPE Indian Oil and Gas Technical Conference and Exhibition, Mumbai, India. https://doi.org/10.2118/113600-MS. SPE-113600-MS.

Solano-Acosta, W., Mastalerz, M., Schimmelmann, A., 2007. Cleats and their relation to geologic lineaments and coalbed methane potential in pennsylvanian coals in Indiana. Int. J. Coal Geol. 72 (3–4), 187–208. https://doi.org/10.1016/j.coal.2007.02.004.

Tan, P., Chen, Z., Huang, L., et al., 2024. Evaluation of the combined in fl uence of geological layer property and in-situ stresses on fracture height growth for layered formations. Pet. Sci. https://doi.org/10.1016/j.petsci.2024.07.014.

Tan, P., Jin, Y., Han, K., et al., 2017. Analysis of hydraulic fracture initiation and vertical propagation behavior in laminated shale formation. Fuel 206, 482–493. https://doi.org/10.1016/j.fuel.2017.05.033.

Tan, P., Jin, Y., Hou, B., et al., 2019. Understanding hydraulic fracture propagation behavior in tight sandstone–coal interbedded formations: an experimental investigation. Petrol. Sci. 1 (16), 148–160. https://doi.org/10.1007/s12182-018-0297-z.

Tan, P., Pang, H.W., Zhang, R.X., et al., 2020. Experimental investigation into hydraulic fracture geometry and proppant migration characteristics for southeastern Sichuan deep shale reservoirs. J. Petrol. Sci. Eng. 184, 106517 https://doi.org/10.1016/j.petrol.2019.106517.

Tan, P., Jin, Y., Wang, Y., et al., 2021. Hydraulic fracture vertical propagation behavior in transversely isotropic layered shale formation with transition zone using XFEM-based CZM method. Eng. Fract. Mech. 248 (16), 107707 https://doi.org/10.1016/j.engfracmech.2021.107707.

Tang, J., Wu, K., Zuo, L., et al., 2019. Investigation of rupture and slip mechanisms of hydraulic fracture in multiple-layered formation. SPE J. 24 (5), 2292–2307. https://doi.org/10.2118/197054-PA.

Unrug, K.F., Thompson, E., Nandy, S., 1985. Evaluation of the Coal Strength for Pillar Calculation Paper Presented at the Society of Mining Engineers Fall Meeting, vol. 280, pp. 2071–2075. Albuquerque, NM, USA.

Wan, L.M., Hou, B., Tan, P., 2019. Observing the effects of transition zone properties on fracture vertical propagation behavior for coal measure strata. J. Struct. Biol. 126, 69–82. https://doi.org/10.1016/j.jsg.2019.05.005.

Wang, H., 2019. Hydraulic fracture propagation in naturally fractured reservoirs: complex fracture or fracture networks. J. Nat. Gas Sci. Eng. 68, 102911 https://doi.org/10.1016/j.jngse.2019.102911.

Wang, X.H., Zhang, F.S., Tang, M.R., 2022. Effect of stress shadow caused by multistage fracturing from multiple well pads on fracture initiation and near- wellbore propagation from infill wells. SPE J. 27 (1), 204–225. https://doi.org/10.2118/208577-PA.

Wei, D., Gao, Z.Q., Fan, T.L., et al., 2017. Experimental hydraulic fracture propagation on naturally tight intra-platform shoal carbonate. J. Petrol. Sci. Eng. 157, 980–989. https://doi.org/10.1016/j.petrol.2017.08.016.

Wu, M.Y., Zhang, D.M., Wang, W.S., et al., 2020. Numerical simulation of hydraulic fracturing based on two-dimensional surface fracture morphology reconstruction and combined finite-discrete element method. J. Petrol. Sci. Eng. 82, 103479 https://doi.org/10.1016/j.jngse.2020.103479.

Zhang, F., Huang, L., et al., 2022. Numerical investigation on the effect of depletion-induced stress reorientation on infill well hydraulic fracture propagation. Pet. Sci. 19, 296–308. https://doi.org/10.1016/j.petsci.2021.09.014.

Zhang, L., Kou, Z., Wang, H., et al., 2018. Performance analysis for a model of a multi-wing hydraulically fractured vertical well in a coalbed methane gas reservoir. J. Petrol. Sci. Eng. 166, 104–120. https://doi.org/10.2118/185172-PA.

Zhao, H., Wang, X., Liu, Z., et al., 2018. Investigation on the hydraulic fracture propagation of multilayers-commingled fracturing in coal measures. J. Petrol. Sci. Eng. 167, 774–784. https://doi.org/10.1016/j.petrol.2018.04.028.

Zheng, Y., He, R., Huang, L., et al., 2022. Exploring the effect of engineering parameters on the penetration of hydraulic fractures through bedding planes in different propagation regimes. Comput. Geotech. 146, 104736. https://doi.org/10.1016/j.compgeo.2022.104736.

Zou, Y.S., Ma, X.F., Zhang, S.C., et al., 2016a. Numerical investigation into the influence of bedding plane on hydraulic fracture network propagation in shale formations. Rock Mech. Rock Eng. 49 (9), 3597–3614. https://doi.org/10.1007/s00603-016-1001-5.

Zou, Y.S., Zhang, S.C., Zhou, T., et al., 2016b. Experimental investigation into hydraulic fracture network propagation in gas shales using CT scanning technology. Rock Mech. Rock Eng. 49 (1), 33–45. https://doi.org/10.1007/s00603-015-0720-3.